Available online at www.sciencedirect.com
SCIENCE DIRECT
Journal of Molecular Catalysis A: Chemical 237 (2005) 182–190
JOURNAL OF MOLECULAR CATALYSIS A: CHEMICAL
www.elsevier.com/locate/molcata

Mesostructured CeO_2 and Pd/CeO_2 nanophases: Templated synthesis, crystalline structure and catalytic properties

J.H. Zhang [a], Y.Q. Yang [a], J.M. Shen [a], J.A. Wang [b,*]

[a] *Chemistry and Chemical Engineering College, Xinyang Normal University, 464000 Xinyang, Henan, PR China*
[b] *Laboratory of Catalysis and Materials, Superior School of Chemical Engineering and Industrial Extractives, National Polytechnic Institute, Col. Zacatenco, C.P. 07738 Mexico City, Mexico*

Received 31 March 2005; accepted 20 April 2005
Available online 6 June 2005

Abstract

This work reports a ceria solid and Pd/ceria catalyst prepared through a surfactant-templated synthesis route used for simultaneous abasement of NO and CO emissions. The surface features, textural properties and crystalline structure of ceria and Pd/ceria catalyst were studied by means of thermogravimetric analysis (TGA), N_2 physisorption isotherms and in situ Fourier transform infrared (FT-IR) spectroscopy, high resolution electron transmission microscopy (TEM) and X-ray diffraction (XRD) techniques. In the calcination procedure, part of the adsorbed water on the surface of the solid was derived into unidentate and bidentate hydroxyls associated with surface cationic ions of ceria. The surfactant cations were strongly interacted with the solid during the preparation, which induces defects formation in the crystalline structure of the annealed ceria. The retained surfactant in the solid could be combusted to yield CO_2, water and organic molecules with a small amount of coke-like deposits. The resultant ceria showed mesoporous texture and cubic phase containing lattice defects in the crystalline structure. The Pd/CeO_2 catalyst was very active for NO reduction via CO with a high selectivity to N_2. A 100% NO conversion with a selectivity to 100% N_2 was achieved over the Pd/ceria catalyst at a reaction temperature of 300 °C. The catalytic activity and selectivity of this catalyst are much superior to the catalysts of Pt or Rh supported on TiO_2, Al_2O_3, TiO_2–Al_2O_3 and ZrO_2–Al_2O_3 prepared by a sol–gel method. A possible reaction mechanism of NO reduction by CO over the Pd/CeO_2 catalyst was discussed.

Keywords: Surfactant-templated synthesis; Pd/ceria; Catalyst; NO reduction; CO oxidation

1. Introduction

A novel synthesis approach of mesoporous Si-MCM-41 materials by using organic molecule as synthetic template reported by Mobil scientists, opens new possibilities in the design of innovative materials with potential applications in a variety of areas [1]. By using similar or modified synthesis route, a number of other metal oxides with mesoporous structures were successfully obtained, these include titania [2], zirconia [3], niobia [4], ceria [5], alumina [6], tin oxide [7] and manganese oxide [8]. Since the enhancement of surface area and controllable porosity, these mesostructured metal oxides are very attractive for catalysis. Among these oxides, ceria is particularly interest in a variety of catalytic processes [9]. For instance, ceria has been used as catalyst or support in the selective oxidation, fine chemicals synthesis, methane steam reforming, phenol hydrogenation at atmospheric pressure and solid oxide fuel cell applications [10–14].

One of the important applications of ceria is the use in the area of environmental catalysis, particularly in the design of the new generation of three-way catalysts for simultaneously controlling NO, CO and hydrocarbon emissions in oxygen-rich conditions. This is because ceria has large oxygen storage capacity and the ability of fast transferring bulk oxygen to its surface [15,16], the former may uptake oxygen

* Corresponding author. Tel.: +52 55 57206000x55124; fax: +52 55 55862728.
E-mail address: jwang@ipn.mx (J.A. Wang).

1381-1169/$ – see front matter © 2005 Elsevier B.V. All rights reserved.
doi:10.1016/j.molcata.2005.04.056

under fuel-lean conditions and the latter may release oxygen under reducing conditions, those allow a ceria-containing catalyst to efficiently work in a relatively wide window of oxygen partial pressure. In addition, ceria may also improve metal dispersion on it and promotes surface and bulk oxygen reducibility of the support when it was used as catalysts additive [17,18]. All of these properties are very important for three-way catalysts for the abatement of automobile exhausts.

Differing from ideas used in the traditional synthesis methods, ceria obtained by using a surfactant-templated synthetic approach shows larger surface area and ordered mesopore structure [5,14]. The mesoporous support of ceria would give rise to stable and well dispersed metal particles on its surface, as a result, enhancement of catalytic performance may be achieved. It is reported that CO conversion on the Pd/ceria prepared by using myristyltrimethylammonium bromide as synthetic template is always higher than that achieved on the one prepared by using a precipitation method, this resulted from larger surface area and better metal dispersion [5].

In the current work, mesoporous ceria nanophase was obtained in a base condition, through a templated synthesis route, using cetyltrimethylammonium chloride as the template. The surface features and texture properties of the resultant ceria are characterized by thermogravimetric analysis (TGA), Fourier transform infrared (FT-IR), Brunaur–Emmett–Teller (BET) and transmission electron microscope (TEM) techniques. Its crystalline structure was refined by applying Rietveld method on the basis of X-ray diffraction (XRD) analysis. Evidence of surfactant association with the pores of the solid is provided and the catalytic activity and selectivity of NO reduction via CO over the ceria and Pd/ceria catalyst are reported.

2. Experimental

2.1. Ceria preparation

To prepare ceria solid, two solutions were prepared: the first solution was prepared by dissolving 16.0 g of cetyltrimethylammonium chloride (CH_3–$(CH_2)_{15}N(CH_3)_3Cl$, referred as CTACl) in 500 ml deionized hot water (around 50 °C) with stirring, followed by adding 120 ml of aqueous ammonia (28 wt.%) to obtain a clear micellar solution; the second solution was prepared by dissolving 21.7 g of $Ce(NO_3)_3{\cdot}6H_2O$ in 500 ml deionized water. The cerium solution was added, drop-by-drop, into the surfactant solution with a proper agitation to disperse the droplets before local concentrations become excessive. The pH value of the mixture remained at approximately 11 in order to induce the hydrolysis and the polycondensation of the inorganic precursor around the formed micelles. Afterwards, the slurry was continuously stirred for 4 h until gel was formed, and then it was sealed in a Teflon bottle for hydrothermal treatment at 100 °C for 5 days. The solid was then filtered and washed with water and methanol for several times. The resultant material was dried at 80 °C for 24 h and then was calcined at 200, 400 and 600 °C for 4 h for further characterization.

2.2. Preparation of 3 wt.% Pd/CeO_2

The 3 wt.% Pd/CeO_2 catalyst was prepared by impregnating the ceria support annealed at 600 °C with a calculated amount of an aqueous solution of $Pd(NO_3)_2{\cdot}2H_2O$. The metal supported catalyst was dried at 120 °C for 4 h and then was calcined at 600 °C for 4 h. Before the catalytic test, the catalyst was reduced by using 99.9% H_2 at 400 °C for 1 h in order to obtain metallic palladium particles on the catalyst.

2.3. Textural properties

The textural properties of the ceria solids were measured in a Digisorb 2405 sorptometer by means of N_2 physisorption isotherms at −195 °C. Before the N_2 adsorption, 0.5 g of the sample was thermally treated at 200 °C under vacuum condition for 6 h in order to remove water from the sample. The surface area was determined according to the standard Brunaur–Emmett–Teller method and the total pore volume was evaluated from the amount of adsorbed N_2 at a relative pressure (P/P_0) of about 0.99. The pore diameter distributions were calculated based on the desorption isotherms by the Barrett–Joyner–Halenda (BJH) algorithm.

2.4. Analysis of thermogravimetric–Fourier transform infrared (TG–FT-IR)

TG analysis was carried out in flow air using a Dupont Model 950 thermoanalyzer from 25 to 800 °C at a heating rate of 20 °C/min to determine weight losses during the thermal treatment and to verify if the CTACl incorporation with the solid materials. The gaseous products produced during TG procedure were simultaneously monitored by means of an on line coupled FT-IR spectroscopic technique.

2.5. Surface characterization by in situ FT-IR

The surface dehydroxylation and removal of the residual surfactants from the dried samples were characterized by using in situ FT-IR spectroscopic technique on a Nicolet Magna-IR 550 spectrometer. The sample was ground by hand with a pestle in a mortar and then pressed at 4 tonnes to give a self-supporting wafer (10 nm in diameter). The sample wafer (around 10 mg) was placed inside an IR cell, which was coupled with a vacuum and heating systems. The sample could be exposed to various gaseous environments with different pressures at different temperatures not exceeding 400 °C. The in situ FT-IR spectra reported herein were recorded at 25, 100, 200, 300 and 400 °C, respectively.

Table 1
Atomic coordinate of the cubic structure with space group *Fm*3*m* (2 2 5)

Atom	Site	*x*	*y*	*z*
Ce	4e	0.00	0.00	0.00
O	4e	0.25	0.25	0.25

2.6. X-ray diffraction analysis and Rietveld refinement

The power X-ray diffraction data were collected at room temperature in a Siemens D-5000 diffractometer with Cu Kα radiation and a secondary beam monochromator. Intensities of the diffraction lines were obtained in the 2θ range between 20° and 110° with a step of 0.02° and a measuring time of 2.5 s at each point. Crystalline structures were refined with the Rietveld technique by using FULLPROF98 code [19]. The atom atomic coordinates used to refine the ceria with cubic structure are reported in Table 1. For the crystalline structure refinement, the solid structure was fitted with a cubic unit cell with space group *Fm*3*m*. The Rietveld refinement provided not only the concentration and average crystallite size of each phase present in the sample but also the lattice parameter and lattice defect information and microstrain in the crystalline structures. The lattice defects were determined by comparing the cation occupancy number with that present in the perfect ideal ceria. The standard deviations, corresponding to the variation of the last significant figures, are given in parentheses. When they correspond to refined parameters, their values are not estimates of the probable error in the analysis as a whole, but only of the minimum possible errors based on their normal distribution.

2.7. Images of transmission electron microscope

High resolution TEM images of CeO_2 and Pd/CeO_2 were carried out in a JEOL 4000 EX electron microscope equipped with a pole piece with spherical aberration coefficient of $C_s = 1.00$ mm. The CeO_2 and Pd/CeO_2 powder samples were grounded softly in an agate mortar and dispersed in isopropyl alcohol in an ultrasonic bath for several minutes. A few drops were then deposited on 200-mesh copper grids covered with a holey carbon film. The electron micrographs were recorded in electron negative films and in a digital PC system attached to the electron microscope. The mean particle diameter (d) was calculated by using the $d = \sum d_i n_i / \sum n_i$ formula, where, n_i is the number of particles and d_i the diameter of the particle i, and the observed particles were arranged by class differing by 0.5 nm in size.

2.8. Catalytic test

The catalytic evaluation of the Pd/ceria for NO reduction by CO was performed on a microreactor system. The reactants mixture fed into the microreactor consisted of 1.5 vol.% CO and 0.5 vol.% NO, the balance was helium. The reactant flow was 30 cm/min and reaction temperature ranged from 50 to 400 °C. Catalyst loading was 50 mg. The effluent discharged from the reactor after the reaction was analyzed by on-line gas chromatography–FT-IR analysis system (HP-5890 Chemical Station and Nicolet-8220 Gas Analyzer). N_2 and CO_2 were analyzed by gas chromatography and CO, N_2O, NO, NO_2 were analyzed by IR. The light-off temperature, T_{50}, is defined as the temperature at which the conversion of CO and NO reaches 50%, respectively.

3. Results and discussion

3.1. Thermal analysis

Fig. 1 shows a TG–DTG profiles of an as-made ceria solid. The temperature range was set between 25 and 900 °C. Two weight loss stages were observed in the TG profile: the first stage ($T < 150$ °C) led to a 2.41 wt.% weight loss that is assigned to desorption of adsorbed water on the sample. The second stage located in the temperature range between 150 and 400 °C which exhibited a maximal rate of weight loss around 3 wt.%/min, showing a pronounced weight loss of 17 wt.%. Above 400 °C, the base line slightly declined down, resulting in a weight loss less than 1 wt.%.

For identifying the gaseous products produced at various weight loss stages in Fig. 1, infrared analysis was simultaneously carried out. Fig. 2 shows a set of FT-IR spectra of the gaseous mixture discharged from the TG system. In the first stage of TG test (<150 °C), the IR spectrum exhibited several groups of peaks: for example, one between 3900 and 3500 cm^{-1} attributed to surface hydroxyls, and another between 1700 and 1300 cm^{-1} (Fig. 2a), these were characteristic of molecular water. This confirms that the first weight loss stage in TG profile is resulted from the desorption of water adsorbed on the sample. It is noted that CO_2 was present in the exit stream because double peaks between 2400 and 2300 cm^{-1} and the ones around 650 cm^{-1} in the IR spectra were formed. Taking into account the fact that the surfactant is thermal stable below 150 °C, obviously, the CO_2 observed in this temperature range was

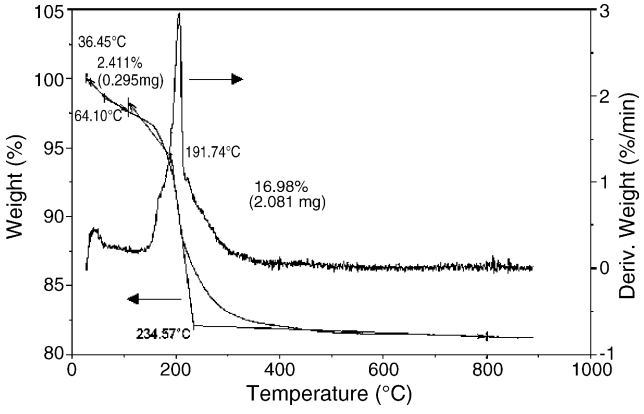

Fig. 1. TG–DTG profiles of the as-prepared ceria dried at 80 °C.

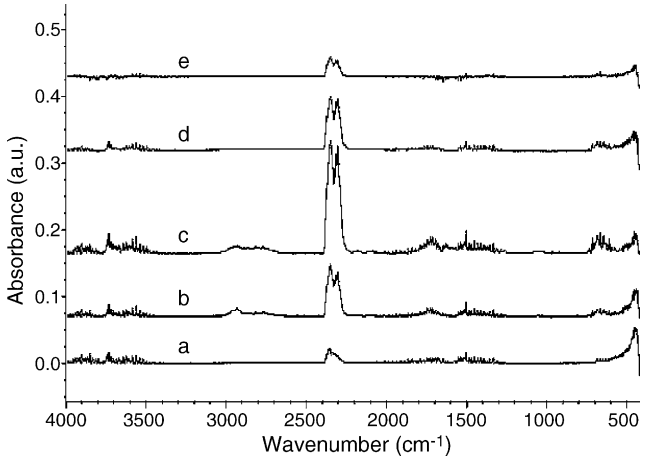

Fig. 2. A set of in situ FT-IR spectra of the exit gases discharged from TG system. The sample used for TG analysis was ceria solid dried at 80 °C. (a) 60 °C; (b) 180 °C; (c) 200 °C; (d) 220 °C; (e) 500 °C.

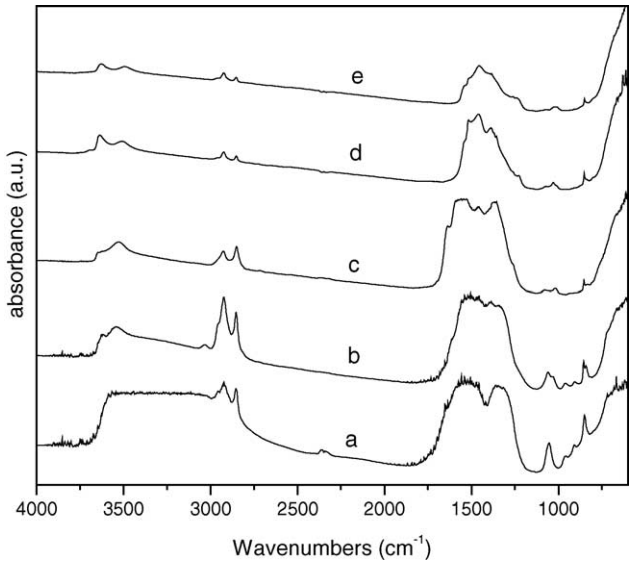

Fig. 3. A set of in situ FT-IR spectra of the as-prepared ceria recorded during the heating procedure in the IR cell. (a) 25 °C; (b) 100 °C; (c) 200 °C; (d) 300 °C; (e) 400 °C.

not produced by surfactant decomposition but likely by the desorption of adsorbed CO_2 on the sample because it was exposed to air before the TG measurement.

In the second weight loss stage (150–400 °C), very sharp IR bands corresponding to CO_2 and H_2O were observed (Fig. 2b–d). The intensities of the bands related to CO_2 greatly increased as the temperature was increased until they reached a maximum at approximately 200 °C. This result indicates that surfactant combustion to produce CO_2 takes place and its burning-off rate increases with increasing of the temperature. Two bands at 2950 and 2800 cm^{-1} were also observed, these are ascribed to the stretching vibration modes of C–H bonds in the hydrocarbon compounds in the outlet gases. Appearance of hydrocarbon compounds also indicates that some residual surfactants were decomposed into small organic molecules and left from the solid to outlet stream. In addition, it is possible, during the synthesis, that polyhydrous cerium oxide $Ce(OH)_x^{(4-x)}{\cdot}yH_2O$ was formed. The decomposition of the hydrous cerium oxide usually occurs in the temperature range between 200 and 300 °C. Therefore, the largest weight loss in the TG profile probably resulted from both the combustion/oxidation of the surfactant and decomposition of hydrous cerium oxide.

In the temperature above 400 °C, CO_2 together with trace water was identified (Fig. 2e). This is likely resulted from the combustion of trace residual coke-like deposits produced by surfactant decomposition.

3.2. Surface characterization by in situ FT-IR

In order to analyze the changes of the ceria surface features during the calcination, in situ FT-IR technique was applied. Fig. 3 shows a set of in situ FT-IR spectra of the as-prepared ceria sample recorded at various temperatures in the IR cell. When the IR spectrum was recorded at 25 °C, a broad absorption band covers the region between 3700 and 3000 cm^{-1}, which is due to water adsorbed on the sample surface. This is in good agreement with the TG-IR characterization shown in Figs. 1 and 2. There are twin bands at 2950 and 2875 cm^{-1}, which are characteristic of the stretching vibrations of C–H bond in hydrocarbons (νCH_{3as} and $\nu(CH_{2as} + \nu CH_{3as})$), i.e., herein the surfactant. In the C–C stretching and C–H deformation vibrations regions, two very tense bands located at approximately 1575 and 1325 cm^{-1}, and the third appeared at 720 cm^{-1}, these peaks are assigned to the vibrations of bending mode (scissoring and rocking vibrations) of the C–H bonds in the groups of $–CH_2–$ and $–CH_3$ in the surfactants [20,21]. It was also observed that a sharp band appeared around 1080 cm^{-1}, it was due to the $(CH_3)_3N–$ group in the surfactant. These observations confirm, once again, that the surfactant cations were indeed strongly interacted with the solid during the preparation, and they were not removed in washing step. In addition, the small double peaks around 2300 cm^{-1} were related to the presence of CO_2. Since the sample was exposed to the air before the IR measurement, it probably adsorbed some CO_2 on the surface, as stated above.

When the temperature in the IR cell was increased to 100 °C, the intensity of the wide band between 3700 and 3000 cm^{-1} was remarkably decreased, and it was replaced by two bands at 3550 and 3625 cm^{-1}. These two bands were attributed to the stretching frequencies of the unidentate (Ce–OH) and bidentate (HO–Ce–OH) species, respectively; while, the double bands corresponding to C–H bonds at 2950 and 2875 cm^{-1} seem to become sharper in comparison with these at 25 °C; however, when the covering effect resulted from the broad peak of the adsorbed water at 25 °C is taken into account, they almost remained unchanged. The bands in the region between 1200 and 1700 cm^{-1} also remained the same as that at 25 °C. These results show that most of the adsorbed water is desorbed, however, the surfactants inside the pores are not yet removed at 100 °C.

As the temperature was raised up to 200 °C, the intensities of the bands around 2800–3000 cm^{-1} clearly reduced and the ones at 1325 and 1575 cm^{-1} were derived into triple bands at 1375, 1460 and 1575 cm^{-1}, with a shoulder at 1630 cm^{-1}. The 1375 and 1575 cm^{-1}, based on the assignments above, they are related to the vibrations of bending modes of the C–H bonds in the groups of $-CH_2-$ and $-CH_3$ in the surfactants. The new one at 1460 cm^{-1} is probably produced by carbonate-like species consideration the surfactant combustion at this temperature [21]. The shoulder band at 1630 cm^{-1} is attributed to flexion vibration of O–H bond. The intensities of the C–H bonds at 1080 and 720 cm^{-1} are also strongly diminished due to the partial removal of the linked surfactant.

When the temperature was increased to 300 and 400 °C, all the bands in the region of 3500–3700 cm^{-1}, 2800–3000 cm^{-1} and 1200–1600 cm^{-1} were further reduced. The one at 1630 cm^{-1} completely disappeared. Since the IR cell could be only performed at temperatures not exceeding 400 °C, further in situ IR characterization at higher temperature was not possible. However, from the information obtained from the TG and FT-IR techniques, the residual coke resulted from the decomposition of surfactant retained on the sample is less than 1 wt.%, which could be removed by calcinations the sample above 600 °C.

3.3. Textural properties

The textural properties of the ceria annealed at 200, 400 and 600 °C were studied by BET method. The values of surface area, mean pore diameter and pore volume are reported in Table 2. Fig. 4 shows the pore diameter distribution and a loop of N_2 adsorption–desorption isotherms of ceria solid annealed at 400 °C. The pore diameter was sharply distributed in a narrow range centered at approximately 3.3 nm at 200 and 400 °C. However, the peak maximum shifted to 7.6 nm when the annealing temperature was increased to 600 °C. With respect to the IUPAC classification [22], the loop of the N_2 adsorption–desorption isotherms belongs to type IV profiles (the inset in Fig. 4). The lack of the sharp steps in both the low relative pressure ($P/P_0 < 0.2$) and the high relative pressure range ($P/P_0 > 0.8$) strongly indicates that this material has no micro- and macropores.

The surface area increased from 150.2 m^2/g at 200 °C to 178.9 m^2/g at 400 °C, and then it decreased to 104.3 m^2/g at 600 °C. This can be explained by the effects of the surfactant

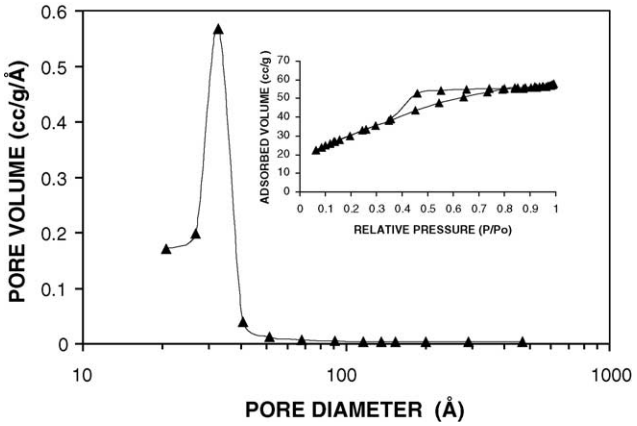

Fig. 4. Pore diameter distribution of the sample calcined at 400 °C. The inserted figure is the loop of N_2 adsorption–desorption isotherms.

incorporation and calcination temperature: at low temperature, i.e., 200 °C, not all the surfactant were removed, some of these species retained in the pores of the solid that may occupy some area. Therefore, the surface area of ceria is relatively lower at this temperature; as the calcination temperature was increased, i.e., to 400 °C, most of the surfactants were burnt off, the surface area reached maximum; further calcination the sample, i.e., at 600 °C, resulted in pore diameter larger, thus lowering the surface area. The surface area is strongly affected by the pore structure in terms of the equation $S = f(V_p/R_p)$, where f is dependent of the pore geometry, and V_p and R_p are the pore volume and pore radius, respectively [23]. Either increasing the pore diameter or decreasing the pore volume or both must lead to the surface area diminishing.

3.4. X-ray diffraction analysis and Rietveld refinement

The crystalline structure of the ceria solid was analyzed by XRD technique and it was carefully refined by the Rietveld method. Fig. 5 shows a Rietveld refinement plot of the Pd/ceria annealed at 600 °C. The XRD analysis shows that the solid contained ceria nanocrystals with pure cubic structure. The crystallite size of ceria was within nanoscale which increased from 7.2 to 19.5 nm as the annealing temperature was raised from 80 to 600 °C (Table 3). Metallic Pd phase was not observed by XRD analysis, indicating that the average crystallite size of Pd was less than 1 nm and the dispersion of the metallic Pd was very high. An interesting result obtained from the structure refinement by the Rietveld method is the formation of many lattice defects in the ceria structure,

Table 2
Textural property of ceria measured by BET method

	Calcination temperature (°C)		
	200	400	600
Surface area (m^2/g)	150.2	178.9	104.3
Mean pore diameter (nm)	3.3	3.3	7.6
Pore volume (cm^3/g)	0.4012	0.3921	0.3748

The sample was annealed at 600 °C.

Table 3
Average crystallite size, lattice parameter, cation occupancy number and defect concentration of CeO_2 obtained by the Rietveld refinement

Average crystallite size (nm)	7.2 (4)	7.3 (1)	19.5 (9)
Lattice cell parameter (nm)	0.5322 (2)	0.5315 (3)	0.5109 (0.7)
Cation occupancy number	0.01843 (11)	0.01926 (6)	0.02004 (2)
Defect concentration (%)	10.9	7.5	3.8

The sample was annealed at 600 °C.

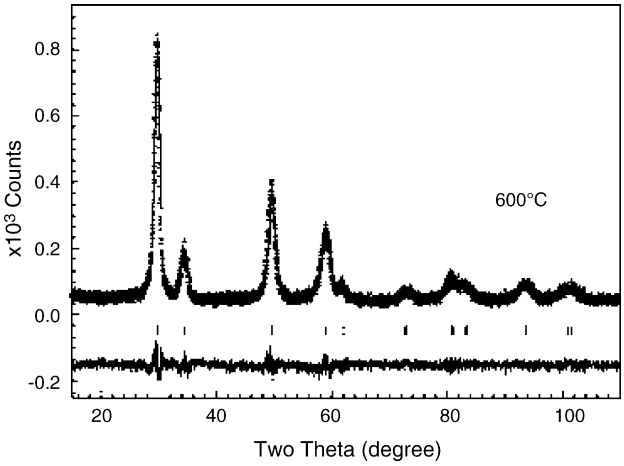

Fig. 5. A Rietveld refinement plot of the Pd/CeO_2 catalyst annealed at 600 °C. Experimental data are indicated by square while the calculated curve obtained after the refinement is indicated with a continuous line. The tick masks correspond to cubic ceria. The continuous curve under the tick marks represents the difference between the experimental and the calculated data. $R_B = 0.11$.

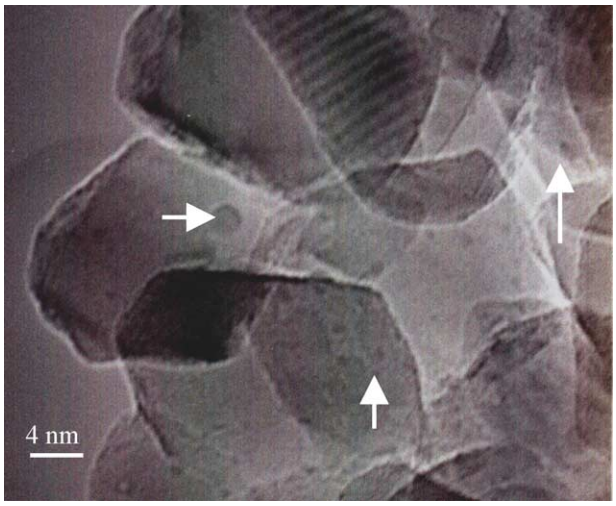

Fig. 6. TEM image of the 3%Pd/ceria sample annealed at 600 °C. The metallic Pd crystals with a size of 0.5–1 nm distributed on the ceria particles were indicated by arrows.

as indicated by the deficiency of the cation occupancy in the crystalline structure. In a perfect ideal ceria crystal with cubic structure, the cation occupancy number is 0.02083, however, as reported in Table 3, the cation occupancy number in the structure of the ceria obtained by the method herein presents a value always less than 0.02083. The defect concentration decreased as the calcination temperature was increased. The degree of crystalline structure imperfection is largely dependent of the surfactant cations incorporation into or removal from the materials that can be explained by a assumed mechanism responsible for phase transformation during the calcination, which may include continuous bond rupture and formation, local temperature rises, microdeformation of the surface and hydrostatic stresses [24,25]. The strong interactions between the deprotonated hydroxyl groups and the positively charged surfactant headgroups, leads to surfactant cationic incorporating within the Ce–O–Ce solid, thus forming a polymeric network of hydrous oxides. Removal of these surfactants at a proper calcination temperature, resulted in defects generation in the corresponding locations of the crystalline structure.

The lattice cell parameter (a) of the ceria slightly decreased when the calcination temperature was increased, indicating a contraction of the lattice cell volume (Table 2). Worth to notice is that the population of the structural defects decreased with increasing of the calcination temperature, too. Therefore, it is possible that formation of the lattice defect enlarges the lattice volume, and when the population of structural defects diminished, the lattice cell trends to shrink to its normal dimension, as observed at 600 °C.

3.5. Morphological features

To study the surface morphology of the Pd/ceria catalyst and to directly observe Pd particles distribution and structural defects in ceria, high resolution TEM technique is applied. The TEM image of the Pd/ceria sample annealed at 600 °C is shown in Fig. 6. Many particles with a size of approximately 20 nm were observed in a Pd/ceria sample, these correspond to ceria crystals. Obviously, the crystalline size observed by TEM image is consistent with the results obtained by the XRD analysis (Table 3). Many nanoclusters with a size between 0.3 and 2 nm, most between 0.5 and 0.9 nm, indicated by white arrows, were also observed, these correspond to metallic palladium crystals distributed on the surface of the ceria particles. The statistical analysis of the dimension of the metallic Pd particles resulted in a very narrow distribution with a mean diameter around $d_m = 0.9$ nm. In Fig. 7, not only lattice point defects but also many lattice line defects located in the crystalline structure of ceria could be observed. It is, once again, in good agreement with the results of the structural defects obtained from the Rietveld refinement and the XRD analyses. It is expected that these structural defects impact on the catalytic properties when ceria is used as catalyst support, which will be further discussed in the following section.

3.6. Catalytic activity and selectivity

Catalytic activity and selectivity of NO reduction by CO over the CeO_2 solid and a Pd/CeO_2 catalyst are reported in Table 4. Above 150 °C of reaction, the bare ceria support could catalyze both reactions of CO oxidation and NO reduction, a selectivity to 100% N_2 was achieved. This result shows that CeO_2 is not an inert support although its catalytic activity is low. When 3 wt.% Pd was loaded on ceria, the catalytic activities for both CO oxidation and NO reduction were remarkably enhanced. The light-off temperature (T_{50}) for CO oxidation and NO reduction was between 100 and 150 °C. N_2O was formed during the reaction, but the

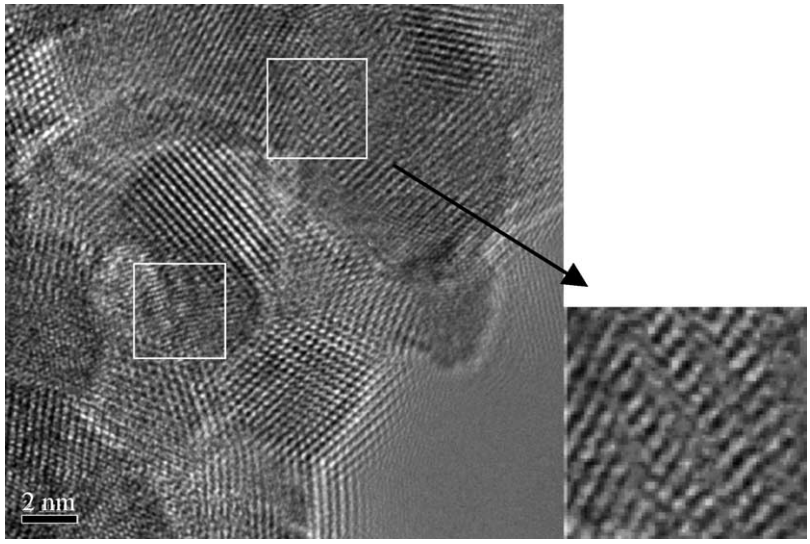

Fig. 7. TEM image of the ceria support annealed at 600 °C. Many structural defects were observed.

Table 4
Activity and selectivity of NO reduction by CO over 3% Pd/CeO_2 catalyst

Temperature (°C)	CO conversion (%)		NO conversion (%)		Selectivity (%)			
	CeO_2	Pd/CeO_2	CeO_2	Pd/CeO_2	CeO_2		Pd/CeO_2	
					N_2	N_2O	N_2	N_2O
50	0	6	0	5	0	0	65	35
100	0	8	0	7	0	0	63	37
150	2	52	1	92	100	0	92	8
200	2	53	2	96	100	0	97	3
250	3	54	3	97	100	0	98	2
300	7	56	5	100	100	0	100	0
350	9	57	5	100	100	0	100	0
400	22	61	8	100	100	0	100	0

selectivity to N_2O strongly depended upon the reaction temperature. It rapidly decreased from 35 to 2% when the reaction temperature was increased from 50 to 250 °C. Above 300 °C, the NO conversion over the Pd/CeO_2 catalyst reached 100%, and the selectivity to N_2 is 100%, too. Increasing reaction temperature probably induces metallic Pd catalyzing the forward reaction of $N_2O + CO \rightleftharpoons N_2 + CO_2$, this accelerates the N_2O decomposition and thus decreases N_2O selectivity, the N_2 selectivity is accordingly enhanced.

In comparison with other catalysts of Pt/Al_2O_3–ZrO_2-SG and Pt/Al_2O_3–TiO_2-SG prepared by a sol–gel method reported by Castillo et al. [26], the Pd/CeO_2 catalyst reported herein shows the highest activity and highest selectivity to N_2 at an identical reaction condition (Table 5). For example, at a reaction temperature of 150 °C, only 19% NO and 17% CO were converted over a 1 wt.% Pt/Al_2O_3–ZrO_2 catalyst and the selectivity to N_2 was 71%. On the 1 wt.% Pt/Al_2O_3–TiO_2-SG catalyst, only 10% of NO was reduced by CO with a N_2 selectivity 69%. While, by using our Pd/ceria catalyst, 92% NO conversion with 92% selectivity to N_2 was achieved.

The Pd/ceria catalyst is also superior to other catalysts of Rh supported sol–gel oxides (Table 6) [27]. Over the 1 wt.% Rh/TiO_2-SG and 1 wt.% Rh/Al_2O_3-SG catalysts, at 200 °C of reaction, the NO conversion was only 4.6 and 3.7% and the selectivity to N_2 was 57 and 60%, respectively. However, at the same reaction condition, 96% of NO was reduced with a selectivity to 97% N_2 over our Pd/CeO_2 catalyst.

It should be pointed out that in the whole reaction temperature range between 50 and 400 °C, NO_2 was not produced at all when NO was reduced by CO over our Pd/ceria catalyst,

Table 5
Comparison of the activity and selectivity of NO reduction by CO over various catalysts tested at 150 °C

Catalysts	Conversion (%)		Selectivity (%)		
	NO	CO	N_2	N_2O	NO_2
3 wt.% Pd/CeO_2	92	52	92	8	0
1 wt.% Pt/Al_2O_3–ZrO_2-SG[a]	19	17	71	21	8
1 wt.% Pt/Al_2O_3–TiO_2-SG[a]	10	20	69	31	0

[a] For detailed information see Ref. [26].

Table 6
Comparison of the activity and selectivity of NO reduction by CO over the various catalysts tested at 200 °C

Catalysts	Conversion (%)		Selectivity (%)		
	NO	CO	N_2	N_2O	NO_2
3 wt.% Pd/CeO_2	96	53	97	3	0
1 wt.% Rh/TiO_2-SG[a]	4.6	4.2	57	39	5
1 wt.% Rh/Al_2O_3-SG[a]	3.7	3.7	60	32	8

[a] For detailed information see Ref. [27].

which is also much better than the two reference groups of catalysts on those NO_2 was usually formed in both conditions with or without oxygen in the reaction mixture.

The difference of the catalytic behaviors between the Pd/ceria herein and the referred catalysts may relate to the defective structure of the ceria support. As shown in Table 2, there are many defects existing in the crystalline structure of ceria. Around these defects, some oxygen ions are not fully bounded and, they are mobile compared to fully bounded ones. These lattice oxygen ions may be released to form free-like oxygen species by breaking the M–O bond when additional energy is supplied. When CO adsorb on the surface of the catalyst where ceria is the support, the free-like oxygen species may transfer from the bulk to surface, to react with the adsorbed CO and yields CO_2, particularly in the case of oxygen absence in the reaction mixture. Therefore, the fast lattice oxygen transport within the ceria is a plausible origin of the low light-off behavior on the Pd/ceria that may lead to oxygen vacancies generation in the bulk of ceria. The other factors, for instance, high metal dispersion achieved on ceria, as observed by TEM and indicated by XRD analysis, may also influence the catalytic behavior and enhances catalytic activity.

In the reduction of NO, metallic Pd takes a key role. First of all, NO might preferentially adsorb on the metallic Pd clusters where it was dissociated, yielding adsorbed N* and O* intermediates [28–30]. The ability of Pd to dissociate the adsorbed NO, from an electronic point of view, might be resulted from the d-electrons from 4d atomic orbital in Pd atoms back-donation to the $2\pi^*$-antibonding orbital of adsorbed NO molecule, that activates the NO–Pd complex and weakens the bond of N–O, and finally it leads to N–O bond destabilization and breaking. Without the metallic Pd, NO dissociation on bare ceria is quilt difficult; therefore, the pure ceria shows low catalytic activity. On the other hand, it is also possible that CO dissociation takes place on the surface of Pd metals to yield C* and O* species. However, in terms of the results reported by Giannakas et al. [31], the energy demanded for NO association with metals is much lower than that for CO association on a variety of catalysts, the energy for NO dissociation is only 60% of that for CO association in both low ($T < 250$ °C) and high ($T > 250$ °C) reaction temperature ranges. Therefore, in the competition of association between NO and CO on the surface of Pd metals, NO association may be dominant. This is in agreement with the fact that conversion of NO is always higher than CO on the same reaction temperature. As a result, CO might preferentially adsorb on the lattice oxygen species, because CO, from the acid–base reaction point of view, is an acidic gas molecule, while, the lattice oxygen ions are usually base sites (electron donors) due to its electron rich character.

Because no any oxygen was supplied from outside the reaction system, oxygen consumed for CO oxidation must come from the ceria support, i.e., surface lattice oxygen and free-like oxygen ion in the defects in the bulk of ceria, and/or oxygen from NO dissociation catalyzed by metallic Pd. Since the population of the surface lattice oxygen and free like oxygen species in the bulk of ceria is limit, the oxygen species produced NO dissociation is mainly responsible for CO oxidation. In this sense, CO conversion is strongly dependent of NO dissociation which is the key step determining CO oxidation. One may image that if the reaction of NO reduced via CO proceeds by a stoichiometric way as $NO + CO = 0.5N_2 + CO_2$, equal molar NO and CO must be consumed, and the CO conversion should be the same as that of NO. However, the experimental data show that NO conversion is always higher than that of CO. The lower CO conversion indicates that the reaction does not follow the stoichiometric pathway. Apart from the effect of association competition of CO and NO taking place on the Pd surface, another possible reason responsible for the low CO conversion is that not all the oxygen species generated from NO dissociation move to the sites where CO are adsorbed, to oxidize CO to CO_2. Some of oxygen species might be stored in oxygen vacancies in the bulk of ceria by forming lattice oxygen.

Based on the above results and discussion, a possible reaction mechanism on NO reduction and CO oxidation over the Pd/ceria catalyst is proposed: in the beginning of the reaction, NO might preferentially adsorb on metallic Pd^0 nanoclusters where the adsorbed NO is dissociated to yield N* and O* intermediates. As the reaction proceeds, the further adsorbed NO might be attacked by the N* intermediate to form N_2 and O* or N_2O. Simultaneously, CO mainly adsorb on the surface lattice oxygen ions (O_L^{2-}) to form $CO - O_L^{2-}$ intermediate species, which further produce CO_2 through a reaction of CO with lattice oxygen, leaving an oxygen vacancy in the corresponding location and two reduced Ce^{3+} ions as neighbors to balance the electrical neutralization of the local structure. The oxygen species around the structural defects in the bulk of ceria may fast move to surface and occupy the surface oxygen vacancies, and oxidize the reduced Ce^{3+} ions to Ce^{4+} ions. Thus, a complete cycle of reduction–oxidation is finished. It is also possible that some of the active O* species might attack the adsorbed CO, yielding CO_2, and other O* species might occupy the surface oxygen vacancies or penetrate into the bulk to occupy the lattice defects, forming lattice oxygen.

4. Conclusions

It has been possible to obtain mesostructured ceria nanophase with structural defects by a surfactant-templated

approach. The strong interaction of the surfactant cations with ceria solid may result in lattice defect formation in the structure of ceria. The retained surfactant could be removed by calcination the sample above 600 °C. The resultant ceria had homogeneous mesopores and single cubic phase with a crystallite size less than 20 nm. When 3 wt.% Pd were dispersed on the surface of ceria, very high metal dispersion was achieved. The 3 wt.% Pd/CeO_2 catalyst showed very high catalytic activity for NO reduction and CO oxidation. Both NO conversion and selectivity to N_2 reached 100% at a reaction temperature of 300 °C. This Pd/ceria catalyst prepared by the method reported herein is much superior to other catalysts where Pt or Rh metals are the active phases and TiO_2, Al_2O_3, Al_2O_3–ZrO_2 and Al_2O_3–TiO_2 prepared by sol–gel method are the support. This work shows that the surfactant-templated method reported herein is very attractive to obtain new materials with specific properties that are difficult by using other technique like sol–gel. The high catalytic activity and excellent selectivity of the Pd/ceria catalyst for NO reduction by CO make it possible to be application in the simultaneous abatement of NO and CO emissions discharged from both the mobile and fixed sources at a moderate temperature.

Acknowledgment

Professor J.A. Wang would like to appreciate the financial support from the projects CONACyT (Grant No. 31282-u), FIES-IMP-IPN (Grant No. 98-29-III) and an international collaboration finding granted by CONACyT (Mexico)-NSF (China) (No. J200.489/2004). The authors thank Dr. M. Morán-Pineda in the Instituto Mexicano del Petroleo and Dr. D.R. Acosta in the National University of Mexico for their valuable technical assistance.

References

[1] C.T. Kresge, M.E. Leonowicz, W.J. Roth, J.C. Vartuli, J.S. Beck, Nature 395 (1992) 710.
[2] D.M. Antonelli, J.Y. Ying, Angew. Chem. Int. Ed. Engl. 34 (1995) 2016.
[3] U. Ciesla, S. Schacht, G.D. Stucky, K.K. Ubger, F. Schüth, Angew. Chem. Int. Ed. Engl. 35 (1996) 541.
[4] D.M. Antonelli, J.Y. Ying, Angew. Chem. Int. Ed. Engl. 35 (1996) 426.
[5] J.A. Wang, J.M. Dominguez, J.A. Montoya, S. Castillo, M. Moran-Pieda, X. Bohkimi, Chem. Mater. 14 (2002) 4676.
[6] F. Vaudry, S. Khodabandeh, M.E. Davis, Chem. Mater. 13 (2000) 1451.
[7] K.G. Severin, T.M. Abdel-Fattah, T.J. Pinnavaia, Chem. Commun. (1998) 1471.
[8] J. Luo, S.L. Suib, Chem. Commun. (1997) 1031.
[9] A. Trovarelli, Catal. Rev. – Sci. Eng. 38 (1996) 439.
[10] T. Chojnscki, K. Krause, L.D. Schimidt, J. Catal. 128 (1991) 161.
[11] H. Idriss, C. Diagne, J.P. Hindermann, A.K. iennemann, M.A. Barteau, J. Catal. 155 (1995) 219.
[12] E.S. Putna, J. Stubenrauch, J.M. Vohs, R.J. Gorte, Langmuir 11 (1995) 4832.
[13] R. Craciun, B. Shereck, R.J. Gorte, Catal. Lett. 51 (1998) 149.
[14] S. Velu, M.P. Kapoor, S. Ingaki, K. Suzuki, Appl. Catal. A: Gen. 245 (2003) 317.
[15] A. Crucq (Ed.), Catalysis and Automotive Pollution Control II, Elseiver Science Publisher, Amsterdam, Oxford, New York, Tokyo, Stud. Surf. Sci. Catal. 71 (1991).
[16] P. Fornasiero, J. Kašpar, M. Graziani, Appl. Catal. B: Environ. 22 (1999) 11–L14.
[17] C.D. Leitenburg, A. Trovarelli, J. Catal. 156 (1995) 171.
[18] D.I. Kondarides, Z.L. Zhang, X.E. Verkios, J. Catal. 176 (1998) 536.
[19] J. Rodríguez-Carbajal, Laboratoire Leon Brillouin (CEA-CNRS), France, Tel.: +33 1 6908 3343, Fax: +33 1 6908 8261, E-mail: juan@llb.saclay.cea.fr.
[20] A. Laachir, V. Perichon, A. Badri, J. Lamotte, E. Catherine, J.C. Lavalley, J. El Fallah, L. Hilarer, F. Le Normand, E. Uenere, G.N. Sauvion, O. Touret, J. Chem. Soc. Faraday Trans. 87 (1991) 1601.
[21] A.V. Ivanov, E. Zausa, Y. Ben Taarit, N. Essayem, Appl. Catal. A: Gen. 256 (2003) 225.
[22] K.S.W. Sing, D.H. Everett, R.A.W. Haul, L. Mousou, R.A. Pierotti, J. Rouquerol, T. Siemieniewska, Pure Appl. Chem. 57 (1985) 57.
[23] A. Lecloux, Comptes-Rendus de La Semaine Detudfe de La Catalyse, vol. 64, Universití de Liége, Eiége, 1970, p. 603.
[24] A. Trovarelli, F. Zamar, J. Llorca, C. De Leitenburg, G. Dolcetti, J.T. Kiss, J. Catal. 169 (1997) 490.
[25] R.M. Davis, B. McDermott, C.C. Koch, Metall. Trans. A 19A (1998) 2867.
[26] S. Castillo, R. Cómez, M. Morán-Pineda, React. Kinet. Catal. Lett. 79 (2) (2003) 271.
[27] S. Castillo, M. Morán-Pineda, V. Molina, R. Cómez, T. López, Appl. Catal. B: Environ. 15 (1998) 203.
[28] S.B. Schwartz, L.D. Schmidt, J. Phys. Chem. 92 (1988) 389.
[29] M. Shelet, G.W. Graham, Catal. Rev. – Sci. Eng. 36 (1994) 433.
[30] J.A. Wang, A. Cuan, J. Salmones, N. Nava, S. Castillo, M. Morán-Pinena, F. Rojas, Appl. Surf. Sci. 230 (2004) 94.
[31] A.E. Giannakas, A.K. Ladavos, P.J. Pomonis, Appl. Catal. B: Environ. 49 (2004) 147.